Endogenous 5-Methylcytosine Protects Neighboring Guanines from N7 and O^6-Methylation and O^6-Pyridyloxobutylation by the Tobacco Carcinogen 4-(Methylnitrosamino)-1-(3-pyridyl)-1-butanone†

Rebecca Ziegel,‡ Anthony Shallop,§ Pramod Upadhyaya,|| Roger Jones,§ and Natalia Tretyakova*,‡,||

Department of Medicinal Chemistry, University of Minnesota School of Pharmacy, Minneapolis, Minnesota 55455, University of Minnesota Cancer Center, Minneapolis, Minnesota 55455, and Department of Chemistry, Rutgers University, Piscataway, New Jersey 08854

Received July 16, 2003; Revised Manuscript Received November 5, 2003

ABSTRACT: All CG dinucleotides along exons 5−8 of the *p53* tumor suppressor gene contain endogenous 5-methylcytosine (^{Me}C). These same sites (e.g., codons 157, 158, 245, 248, and 273) are mutational hot spots in smoking-induced lung cancer. Several groups used the UvrABC endonuclease incision assay to demonstrate that methylated CG dinucleotides of the *p53* gene are the preferred binding sites for the diol epoxides of bay region polycyclic aromatic hydrocarbons (PAH). In contrast, effects of endogenous cytosine methylation on the distribution of DNA lesions induced by tobacco-specific nitrosamines, e.g., 4-(methylnitrosamino)-1-(3-pyridyl)-1-butanone (NNK), have not been elucidated. In the work presented here, a stable isotope labeling HPLC−ESI-MS/MS approach was employed to analyze the reactivity of the N7 and O^6 positions of guanines within hemimethylated and fully methylated CG dinucleotides toward NNK-derived methylating and pyridyloxobutylating species. $^{15}N_3$-labeled guanine bases were placed within synthetic DNA sequences representing endogenously methylated *p53* codons 154, 157, and 248, followed by treatment with acetylated precursors to NNK diazohydroxides. HPLC−ESI-MS/MS analysis was used to determine the relative yields of N7- and O^6-guanine adducts at the $^{15}N_3$-labeled position. In all cases, the presence of ^{Me}C inhibited the formation of N7-methylguanine, O^6-methylguanine, and O^6-pyridyloxobutylguanine at a neighboring G, with the greatest decrease observed in fully methylated dinucleotides and at guanines preceded by ^{Me}C. Furthermore, the O^6-Me-dG/N7-Me-G molar ratios were decreased in the presence of the 5′-neighboring ^{Me}C, suggesting that the observed decline in O^6-alkylguanine adduct yields is, at least partially, a result of an altered reactivity pattern in methylated CG dinucleotides. These results indicate that, unlike N^2-guanine adducts of PAH diol epoxides, NNK-induced N7- and O^6-alkylguanine adducts are not preferentially formed at the endogenously methylated CG sites within the *p53* tumor suppressor gene.

In mammalian genomic DNA, 3−5% of the cytosine residues are present as 5-methylcytosine (^{Me}C)[1] within CG dinucleotides (*1*−*3*). Endogenous methylation of CG sequences in promoter regions is usually associated with gene silencing (*4*, *5*), supposedly a result of ^{Me}C-associated effects on protein binding, histone acetylation status, and chromatin structure (*6*, *7*). Recent investigations have established a link between cytosine methylation and mutagenesis and/or carcinogenesis (*5*, *7*−*9*). Promoter regions of many cancer-related genes, including tumor suppressor genes, genes that suppress metastasis and angiogenesis, and DNA repair genes, are characterized by an aberrant or accidental methylation in cancer (*5*, *8*).

All CG sites along exons 5−8 of the *p53* tumor suppressor genes contain ^{Me}C (*10*). While the biological function of this methylation is unknown, these sites are frequently mutated in human cancer, e.g., mutational hot spots at *p53* codons 157, 158, 245, 248, and 273 in lung cancer (*11*), codons 175, 245, 248, 273, and 282 in colon cancer (*12*), and codons 175, 248, 273, and 282 in breast cancer (*12*, *13*). Some of these genetic changes can be rationalized by the hydrolytic deamination of ^{Me}C to thymine, giving rise to CG → TA transitions (*12*, *14*−*17*). However, in lung cancer, the mutations observed at the ^{Me}CG sites are primarily G → T transversions (*11*, *12*, *18*−*20*). Point mutations at the CG dinucleotides of the *p53* gene are characteristic for lung cancer and are found more frequently in tumors of smokers

† Funding for this research was from the University of Minnesota Department of Medicinal Chemistry, University of Minnesota Cancer Center, and the National Cancer Institute (Grant CA095039).

‡ University of Minnesota School of Pharmacy.

§ Rutgers University.

|| University of Minnesota Cancer Center.

[1] Abbreviations: AGT, O^6-alkylguanine DNA alkyltransferase; BPDE, benzo[*a*]pyrene diol epoxide; DMS, dimethyl sulfate; D_3-O^6-Me-dG, D_3-O^6-methyl-2′-deoxyguanosine; HPLC−ESI-MS/MS, HPLC−electrospray ionization tandem mass spectrometry; ^{Me}C, 5-methylcytosine; MNNG, *N*-methyl-*N*′-nitronitrosoguanidine; MNU, *N*-nitroso-*N*-methylurea; N7-Me-G, N7-methylguanine; NDMAOAc, (acetoxymethyl)methylnitrosamine; NNK, 4-(methylnitrosamino)-1-(3-pyridyl)-1-butanone; NNKOAc, 4-[(acetoxymethyl)nitrosamino]-1-(3-pyridyl)-1-butanone; O^6-Me-G, O^6-methylguanine; O^6-Me-dG, O^6-methyl-2′-deoxyguanosine; O^6-POB-G, O^6-[4-oxo-4-(3-pyridyl)but-1-yl]guanine; O^6-POB-dG, O^6-[4-oxo-4-(3-pyridyl)but-1-yl]deoxyguanosine; PAH, polycyclic aromatic hydrocarbons; POB, 4-oxo-4-(3-pyridyl)but-1-yl; SPE, solid phase extraction; SRM, selected reaction monitoring.

10.1021/bi035259j CCC: $27.50
Published on Web 12/20/2003

Scheme 1: Metabolic Activation of NNK to DNA Reactive Species To Produce Methylated and Pyridyloxobutylated Guanine Adducts

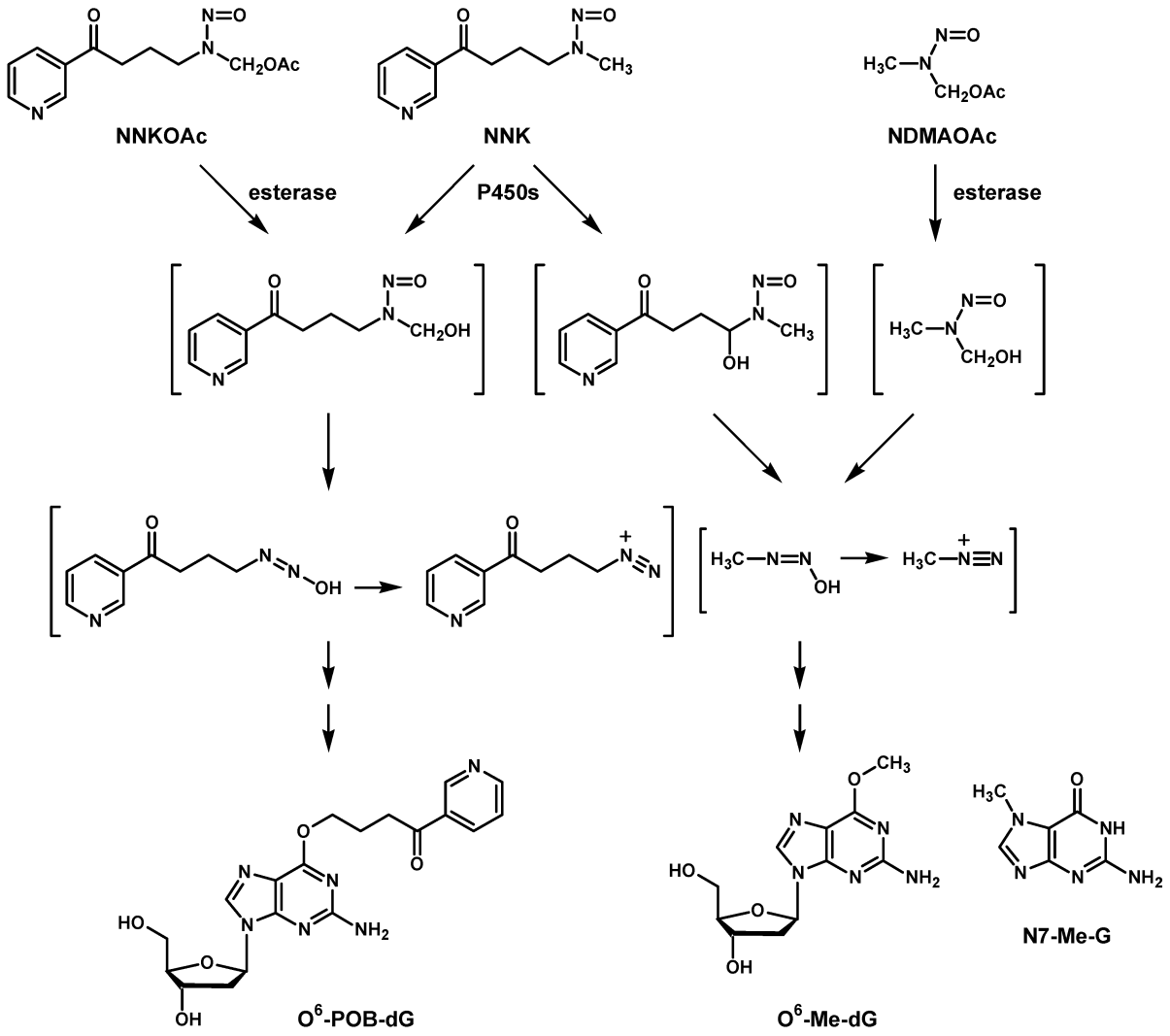

than in nonsmokers, suggesting a role of tobacco carcinogens or other exogenous factors in these genetic changes (*12*, *19*−*21*).

One possible explanation for the observed "hypermutability" of the methylated *p53* CG sites in smoking-induced lung cancer involves an increased reactivity of guanine nucleobases within ^{Me}CG dinucleotides toward tobacco carcinogens (*22*). Indeed, the presence of ^{Me}C in CG dinucleotides has been shown to stimulate guanine adduct formation by several carcinogens, e.g., diol epoxide metabolites of polycyclic aromatic hydrocarbons (PAH) (*22*, *23*), aflatoxin B_1 8,9-epoxide (*24*), and *N*-acetoxy-2-acetylaminofluorene (*24*). The antitumor agents mitomycin C, mitoxantrone, and esperamicins A1 and C also demonstrate an increased reactivity at these locations (*25*−*27*). In contrast, bleomycin-mediated strand scission and guanine alkylation by *N*-methyl-*N*-nitrosourea and *N*-ethyl-*N*-nitrosourea are inhibited in the presence of ^{Me}C (*28*−*30*).

This study examines the effects of neighboring ^{Me}C on the reactivity of guanine nucleobases toward tobacco-specific nitrosamine 4-(methylnitrosamino)-1-(3-pyridyl)-1-butanone (NNK, Scheme 1). DNA alkylation by NNK-derived methyldiazohydroxide and [4-oxo-4-(3-pyridyl)but-1-yl]-diazohydroxide gives rise to multiple adducts, including N7-methyl-2′-deoxyguanine (N7-Me-dG), O^6-methyl-2′-deoxyguanosine (O^6-Me-dG), and O^6-[4-oxo-4-(3-pyridyl)but-1-yl]deoxyguanosine (O^6-POB-dG, Scheme 1) (*31*). While N7-Me-dG lesions are by far the most abundant, O^6-substituted guanines are highly mispairing (*32*). In site-specific mutagenesis studies, O^6-Me-dG and O^6-POB-dG produce high levels of G → A transition mutations (*33*, *34*), while O^6-POB-dG also leads to a small number of G → T transversions (*34*). In addition, pyridyloxobutyl (POB) adducts (e.g., O^6-POB-dG) inhibit O^6-alkylguanine DNA alkyltransferase (AGT)-mediated repair of O^6-Me-dG adducts, potentially increasing their persistence *in vivo* (*35*−*37*). In support of the role of these lesions in tobacco mutagenesis, previous studies have observed a correlation between the formation of O^6-Me-dG adducts and lung tumor multiplicity in NNK-treated rats and mice (*38*, *39*). N7-Me-dG adducts are not mispairing, but can undergo spontaneous depurination ($t_{1/2}$ = 80−160 h) to produce the corresponding free bases (N7-Me-G) and abasic sites in DNA (*32*, *40*). If not repaired, abasic sites can cause G → T transversions (*41*−*44*).

In the work presented here, we have employed a stable isotope labeling HPLC−MS/MS method (Scheme 2) (*45*, *46*) to follow the formation of N7-Me-dG, O^6-Me-dG, and O^6-POB-dG at specific guanine bases in the *p53* sequence

Scheme 2: Strategy for the Quantitation of NNK−Guanine Adducts at Specific Guanines within a Region of the *p53* Gene

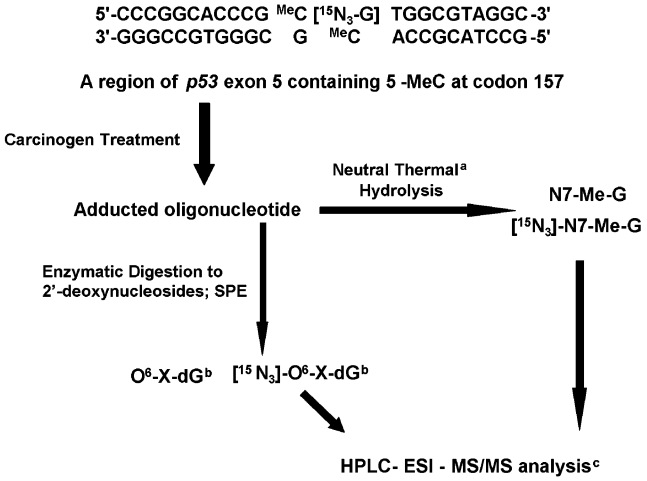

[a] Neutral thermal hydrolysis was not performed on NNKOAc-treated oligonucleotides. [b]X is Me for NDMAOAc-treated oligonucleotides and POB for NNKOAc-treated oligonucleotides. [c]N7-Me-G adducts were analyzed using HPLC−ESI-MS.

context both in the absence and in the presence of the 5-methyl substituents at neighboring cytosines. Acetylated precursors of methyl and pyridyloxobutyl diazohydroxides (NMDAOAc and NNKOAc, respectively, Scheme 1) were employed to model DNA methylation and pyridyloxobutylation by NNK metabolites. Our main goal was to analyze the effects of endogenous cytosine C5 methylation on NNK-induced guanine adduct formation within the *p53* tumor suppressor gene and to determine a possible mechanism for this effect.

MATERIALS AND METHODS

Warning

(Acetoxymethyl)methylnitrosamine (NDMAOAc) and 4-[(acetoxymethyl)nitrosamino]-1-(3-pyridyl)-1-butanone (NNKOAc) are carcinogenic and mutagenic in laboratory animals and should be handled with extreme caution (*47*).

Materials

NDMAOAc was purchased from the NCI Chemical Carcinogen Repository (Midwest Research Institute, Kansas City, MO). NNKOAc was synthesized as previously reported (*36*). O^6-POB-dG was a gift from Prof. Lisa Peterson at the University of Minnesota Cancer Center. Deuterated methanol was obtained from Aldrich (Milwaukee, WI). Diisopropyl azodicarboxylate was purchased from Acros Organics, Fisher Scientific (Fair Lawn, NJ). N7-Me-G and O^6-Me-dG standards were purchased from Sigma (St. Louis, MO). DNA oligomers containing ^{Me}C and $^{15}N_3$-dG at specified locations (Table 1) were prepared by standard phosphoramidite chemistry using a DNA synthesizer at the University of Minnesota Microchemical Facility (Minneapolis, MN). The 1,7-NH_2-^{15}N-dG phosphoramidite was prepared at Rutgers University as described elsewhere (R. Jones and A. Shallop, manuscript in preparation). ^{Me}C phosphoramidite was purchased from Glen Research Corp. (Sterling, VA). In each oligomer, $^{15}N_3$-dG and ^{Me}C were placed at the specified positions as shown in Table 1.

Table 1: *p53* Gene Sequences Used To Determine the Effect of ^{Me}C on the Reactivity of Specific Guanines toward Activated NNK Metabolites (G is $^{15}N_3$-dG)

***p53* codons 151-156:**	
5'-CCCCCGCC **CG** GCACCCGC-3'	5'-CCCCCGCC **C G** GCACCCGC-3'
3'-GGGGGCGG **GC** CGTGGGCG-5'	3'-GGGGGCGG **G^{Me}C** CGTGGGCG-5'
5'-CCCCCGCC **^{Me}CG** GCACCCGC-3'	5'-CCCCCGCC **^{Me}C G** GCACCCGC-3'
3'-GGGGGCGG **GC** CGTGGGCG-5'	3'-GGGGGCGG **G^{Me}C** CGTGGGCG-5'
***p53* codons 153-158:**	
5'-CCCGGCACCCG **CG** TCCGCG-3'	5'-CCCGGCACCCG **C G** TCCGCG-3'
3'-GGGCCGTGGGC **GC** AGGCGC-5'	3'-GGGCCGTGGGC **G^{Me}C** AGGCGC-5'
5'-CCCGGCACCCG **^{Me}CG** TCCGCG-3'	5'-CCCGGCACCCG **^{Me}C G** TCCGCG-3'
3'-GGGCCGTGGGC **GC** AGGCGC-5'	3'-GGGCCGTGGGC **G^{Me}C** AGGCGC-5'
***p53* codons 246-251:**	
5'-CATGAAC **CG** GAGGCCCATC-3'	5'-CATGAAC **C G** GAGGCCCATC-3'
3'-GTACTTG **GC** CTCCGGGTAG-5'	3'-GTACTTG **G^{Me}C** CTCCGGGTAG-5'
5'-CATGAAC **^{Me}CG** GAGGCCCATC-3'	5'-CATGAAC **^{Me}C G** GAGGCCCATC-3'
3'-GTACTTG **GC** CTCCGGGTAG-5'	3'-GTACTTG **G^{Me}C** CTCCGGGTAG-5'

D_3-O^6-Methyl-2′-deoxy-N^2-isobutyrylguanosine 3′,5′-Diisobutyrate. D_3-O^6-Me-dG was prepared by a modification of a previously published method for O^6-POB-dG (*48*). The synthesis of the protected precursor to D_3-O^6-Me-dG, D_3-O^6-methyl-2′-deoxy-N^2-isobutyrylguanosine 3′,5′-diisobutyrate, was initiated by drying triphenylphosphine (0.75 mmol, 197 mg) and 2′-deoxy-N^2-isobutyrylguanosine 3′,5′-diisobutyrate (0.5 mmol, 239 mg) together under vacuum for 72 h and dissolving them in anhydrous 1,4-dioxane (10 mL) containing deuterated methanol (0.75 mmol, 34 μL). Diisopropyl azodicarboxylate (0.75 mmol, 148 μL) in anhydrous 1,4-dioxane (2 mL) was then added dropwise. The reaction mixture was purged with nitrogen and stirred for 20 h at room temperature. Dichloromethane (250 mL) was added, and the mixture was washed three times with water. The organic phase was dried over magnesium sulfate, filtered, and concentrated under reduced pressure. D_3-O^6-Methyl-2′-deoxy-N^2-isobutyrylguanosine 3′,5′-diisobutyrate was purified by preparative TLC (Whatman silica gel plates, 150 Å, 1000 μm thick) using 30% dichloromethane in ethyl acetate.

D_3-O^6-Me-dG. D_3-O^6-Methyl-2′-deoxy-N^2-isobutyrylguanosine 3′,5′-diisobutyrate was dissolved in a 1:1 mixture of 2 M sodium hydroxide and methanol (20 mL) and hydrolyzed at room temperature for 3 h. The reaction mixture was neutralized by the addition of 95% acetic acid. D_3-O^6-Me-dG was extracted with ethyl acetate (25 mL), and the mixture was washed three times with water (100 mL). The organic layer was dried over magnesium sulfate, filtered, and concentrated under reduced pressure. D_3-O^6-Me-dG was purified by HPLC using a Supelcosil LC-18-DB column (4.6 mm × 250 mm, 5 μm) eluted with a gradient of 150 mM ammonium acetate (A) and acetonitrile (B), at a flow rate of 1 mL/min. The percentage of B was increased from 2 to 15.5% over the course of 15 min. HPLC−MS/MS analysis of the synthetic D_3-O^6-Me-dG [*m*/*z* 285.1, $(M + H)^+$] revealed that it coeluted with the authentic O^6-Me-dG: MS/MS *m*/*z* 285.1 [$(M + H)^+$] → 169.1 ($M + H - dR$); ^{1}H NMR (500 MHz, d_6-DMSO) δ 8.1 (s, 1H, H-8), 6.42 (s, 2H, NH_2), 6.21 (dd, 1H, $J_{1'-2'} = 7.5$ Hz, $J_{1'-2''} = 6.2$ Hz,

H-1′), 5.25 (m, 1H, CHO**H**-3′), 5.0 (m, 1H, CHO**H**-5′), 4.38 (m, 1H, H-3′), 3.6 (m, 1H, H-4′), 3.4 (m, 1H, H-5′), 2.2 (m, 1H, H-2′), 2.1 (m, 1H, H-2″).

D_3-N7-Me-G. 2′-dG [5 mM in 10 mM Tris-HCl buffer (pH 7)] was reacted with d_6-dimethyl sulfate (100 mM) at 37 °C for 6 h. The reaction mixture was separated by HPLC with an Agilent Eclipse XDB-C8 column (4.6 mm, 5 μm) eluted at a flow rate of 1 mL/min. The HPLC solvents were 15 mM ammonium acetate (pH 5.5) (A) and 100% ACN (B). The mobile phase was maintained at 0% B for the first 3 min, followed by a linear gradient from 0 to 40% B over the course of 18 min. Under these conditions, D_3-N7-Me-G eluted as a sharp peak at 7.8 min.

Purification of DNA Strands

All DNA oligodeoxynucleotides employed in this work (Table 1) were carefully purified by reversed phase HPLC using an Agilent Technologies 1100 system. A semipreparative Supelcosil LC-18-DB column (Supelco, Bellefonte, PA) was maintained at 40 °C and eluted at a flow rate of 3 mL/min. The HPLC eluent was analyzed with a UV detector set to 260 nm. Chromatographic solvents consisted of 100 mM triethylammonium acetate (pH 7) (A) and 50% acetonitrile in 100 mM triethylammonium acetate (pH 7) (B). The mobile phase was linearly changed from 7.5 to 26% B over the course of 42 min, and then increased to 34% B in the remaining 18 min. Fractions corresponding to the full-length oligomers were collected and concentrated under vacuum. The identity of each strand was confirmed by ESI-MS analysis with an Agilent 1100 capillary LC−ion trap MS system. DNA purity was established by HPLC with a different solvent system. A Supelcosil LC-18-DB column (2.1 mm × 250 mm, 5 μm, Supelco) was eluted with 150 mM ammonium acetate (A) and acetonitrile (B) at a gradient of 5 to 12% B over the course of 40 min. DNA was considered pure if the impurity peaks in the HPLC traces constituted less than 2% of the total area. Quantification of purified DNA strands was performed by UV spectrophotometry using the calculated values of the molar extinction coefficients [ϵ = 157 109 for (+) *p53* codon 154, ϵ = 157 459 for (+) *p53* codon 154-Me, ϵ = 190 114 for (−) *p53* codon 154, ϵ = 190 464 for (−) *p53* codon 154-Me, ϵ = 174 703 for (+) *p53* codon 157, ϵ = 175 053 for (+) *p53* codon 157-Me, ϵ = 196 695 for (−) *p53* codon 157, ϵ = 197 045 for (−) *p53* codon 157-Me, ϵ = 204 206 for (+) *p53* codon 248, ϵ = 204 356 for (+) *p53* codon 248-Me, ϵ = 193 199 for (−) *p53* codon 248, and ϵ = 193 549 for (−) *p53* codon 248-Me]. Equimolar amounts of the complementary DNA strands were annealed as previously described (*45*, *46*). Duplex formation under these conditions was complete as determined by nondenaturing HPLC.

DNA Methylation and Hydrolysis (Scheme 2)

Double-stranded oligodeoxynucleotides (3−4 nmol) containing $^{15}N_3$-dG and ^{Me}C at the specified CG site within *p53*-derived sequences (Table 1) were treated with (acetoxymethyl)methylnitrosamine (NDMAOAc) (2 mM) in the presence of esterase as described previously (*46*). The reaction was stopped by the ethanol precipitation of DNA. The methylated DNA was dissolved in water, and the N7-Me-G and $^{15}N_3$-N7-Me-G lesions were released as free bases by heating at 95 °C for 30 min. The partially depurinated DNA backbone was precipitated with cold ethanol. The supernatant was dried under vacuum, and N7-Me-G adducts were dissolved in 20 μL of 15 mM ammonium acetate; 4 μL of a sample solution was injected onto a capillary HPLC system for HPLC−ESI-MS analysis as described below (Scheme 2) (*46*).

The remaining DNA pellet was dissolved in 10 mM Tris-HCl buffer (pH 7.0), containing 15 mM $MgCl_2$, and enzymatically hydrolyzed to deoxynucleosides by incubation with 30 units of DNase I (30 min, 37 °C), followed by the addition of phosphodiesterase I (100 milliunits) and alkaline phosphatase (8 units) in 50 mM Tris/15 mM $MgCl_2$ buffer (pH 9.3) and an additional incubation at 37 °C for 18 h (Scheme 2). Aliquots were removed for HPLC analysis to ensure complete digestion. O^6-Me-dG and $^{15}N_3$-O^6-Me-dG adducts were isolated by solid phase extraction using Strata-X SPE cartridges (Phenomenex, Torrance, CA) eluted with a step gradient of methanol in water. The 50% methanol fraction containing O^6-Me-dG adducts was dried under vacuum and redissolved in 20 μL of 15 mM ammonium acetate; 4−8 μL of the sample was used for capillary HPLC−ESI-MS/MS analyses as described below.

DNA Pyridyloxobutylation and Hydrolysis (Scheme 2)

Double-stranded DNA oligomers representing a region of the *p53* gene surrounding codon 157 with different C methylation status (Table 1, 5 nmol each) were treated with NNKOAc (5 mM) in the presence of esterase for 90 min (*46*). All treatments were performed in quadruplicate. Following enzymatic hydrolysis of DNA to 2′-deoxynucleosides in the presence of micrococcal nuclease (1.2 units), phosphodiesterase II (22 milliunits), and alkaline phosphatase (8.2 units) (*46*), aliquots were removed and checked by HPLC to ensure complete digestion. O^6-POB-dG adducts were isolated by solid phase extraction using Strata-X SPE cartridges (Phenomenex) sequentially eluted with a 50% methanol/water mixture and 100% methanol. The 100% methanol fraction containing O^6-POB-dG was dried under vacuum and redissolved in 20 μL of 15 mM ammonium acetate containing 10% acetonitrile; 8 μL of a sample solution was injected onto the HPLC system for capillary HPLC−ESI-MS/MS analyses as described below.

HPLC−ESI-MS/MS Analyses of Methylated and Pyridyloxobutylated Lesions

N7-Me-G. The HPLC−ESI-MS analysis of N7-Me-G was performed with an Agilent 1100 capillary LC−ion trap MS system. Chromatographic separation was achieved with a Zorbax SB-C18 column (150 mm × 0.5 mm, 5 μm, Agilent Technologies) maintained at 20 °C and eluted at a flow rate of 15 μL/min with 15 mM ammonium acetate (pH 5.5) (A) and 100% acetonitrile (B). The mobile phase was maintained at 0% B for the first 3 min and changed to 20% B over the next 13.5 min, and the organic fraction was further increased to 40% B over the remaining 2.5 min. The mass spectrometer was tuned to maximum sensitivity by directly infusing the N7-Me-G standard solutions. The instrument was operated in the positive ion mode with nitrogen as a nebulizing and drying gas (15 psi, 5 L/min). The drying gas temperature was set to 200 °C. Quantitative analysis of N7-Me-G was

achieved by full-scan HPLC−ESI-MS with a scan range of *m*/*z* 140−180. The typical target ion abundance value was set to 50 000, and the maximum accumulation time was 50 ms. Extracted ion chromatograms (*m*/*z* 166.0 for N7-Me-G and *m*/*z* 169.0 for [$^{15}N_3$]N7-Me-G) were used for quantification.

Standard solutions containing known amounts of N7-Me-G and D_3-N7-Me-G were injected to ensure that HPLC−MS peak area ratios for *m*/*z* 166.0 and 169.0 were consistent with the actual molar ratios of N7-Me-G and D_3-N7-Me-G. Calibration curves were constructed by injecting known amounts of each standard, followed by linear regression analysis of HPLC−ESI-MS/MS peak area versus adduct concentration (typical $R^2 = 0.990-0.997$).

O6-Me-dG. An Agilent 1100 capillary LC−ion trap mass spectrometer (Agilent Technologies) was operated in the ESI^+ mode. Chromatographic separation was achieved with a Zorbax SB-C18 column (150 mm × 0.5 mm, 5 μm, Agilent Technologies) eluted at a flow rate of 15 μL/min with a gradient of 15 mM ammonium acetate (pH 5.5) (A) and 100% acetonitrile (B). The solvent composition was linearly changed from 0 to 13% over the course of 27 min, and then the organic fraction was raised to 60% over the next 6 min, and further to 100% in the remaining 7 min. Nitrogen was used as a nebulizing (15 psi) and drying gas (5 L/min, 200 °C). The instrument was tuned to maximum sensitivity by directly infusing the O^6-Me-dG standard. Quantitative analysis was achieved by monitoring the MS/MS transitions corresponding to the loss of deoxyribose from O^6-Me-dG (*m*/*z* 282.1 → 166.1) and $^{15}N_3$-O^6-Me-dG (*m*/*z* 285.1 → 169.1). The target ion abundance value was set to 50 000; the maximum accumulation time was 300 ms, and three scans were taken on average. A typical fragmentation amplitude was 0.9 V, with a scan width of 1.2 amu. HPLC−MS/MS analysis of standard mixtures containing known molar ratios of O^6-Me-dG and D_3-O^6-Me-dG ensured that the isotopomers could be resolved and accurately quantified by our methods. Calibration curves were constructed by injecting known amounts of each standard, followed by linear regression analysis of the HPLC−ESI MS/MS peak area versus adduct concentration (typical $R^2 = 0.994-0.998$).

O^6-POB-dG. An Agilent 1100 capillary LC−ion trap system was used in these experiments. A Zorbax SB-C18 column (150 mm × 0.5 mm, 5 μm, Agilent Technologies) was eluted at a flow rate of 15 μL/min with 15 mM ammonium acetate (A) and 100% acetonitrile (B). A linear gradient from 10 to 30% B over the course of 32 min was employed. The mass spectrometer was tuned to maximize sensitivity by directly infusing a standard solution of O^6-POB-dG. The instrument was operated in the ESI^+ mode with nitrogen as a nebulizing (15 psi) and drying gas (5 L/min, 200 °C). Quantitative analysis of O^6-POB-dG was achieved by monitoring the *m*/*z* 415.4 → 299.1 and *m*/*z* 418.4 → 302.1 transitions corresponding to the loss of deoxyribose from the $[M + H]^+$ ions of O^6-POB-dG and $^{15}N_3$-O^6-POB-dG, respectively. A typical fragmentation amplitude was 0.9 V, with a scan width of 1.2 amu. The target ion abundance value was set to 30 000; the maximum accumulation time was 300 ms, and three scans were taken per average. Standard solutions containing known amounts of unlabeled and D_3-labeled O^6-POB-dG were injected prior to sample analyses to confirm that the ratios of HPLC−MS/MS peak areas accurately reflected the relative concentrations of the two isotopomers.

RESULTS

Selection of DNA Sequences. Synthetic oligomers representing *p53* regions containing codons 154, 157, and 248 (Table 1) were used to establish the effect of ^{Me}C on the production of NNK adducts at the neighboring guanine (Table 1). Codons 157 and 248 are among *p53* mutational "hot spots" observed in smoking-induced lung cancer (*11*, *19*), while codon 154 is usually unaffected. The extent of adduct formation at specific guanine bases within CG sites was determined by the previously described stable isotope labeling HPLC−ESI-MS/MS approach (*45*, *46*). In brief, $^{15}N_3$-labeled guanine was inserted at a specific location within *p53* gene-derived synthetic oligodeoxynucleotides with defined cytosine methylation status (Table 1). Following treatment with the methylating agent (NDMAOAc) or the pyridyloxobutylating agent (NNKOAc) and hydrolysis of the DNA duplexes, the alkylated nucleobases or nucleosides were quantified by HPLC−ESI-MS/MS (Scheme 2). Because the molecular weights of nucleobase adducts originating from the labeled site are increased by three mass units as a result of the $^{15}N_3$ label, the extent of adduct formation at that site can be established by mass spectrometry. To independently examine the effects of base-paired ^{Me}C and 5′-neighboring ^{Me}C, methylated cytosine was placed in either one or both DNA strands (Table 1). The extent of adduct formation in the presence of ^{Me}C was normalized to the adduct yields at the same guanine in the absence of ^{Me}C (100%).

5′-Neighboring ^{Me}C Inhibits O^6-Me-dG Adduct Formation at the Target Guanine. Figure 1 illustrates HPLC−ESI-MS/MS analysis of O^6-Me-dG and $^{15}N_3$-O^6-Me-dG originating from a double-stranded DNA 19-mer following NMDAOAc treatment. Signals specific to O^6-Me-dG and $^{15}N_3$-O^6-Me-dG are observed in the corresponding ion channels (*m*/*z* 282.1 → 166.1 and *m*/*z* 285.1 → 169.1, respectively, Figure 1). Shaded peaks in the bottom panel represent $^{15}N_3$-O^6-Me-dG lesions that originate from the $^{15}N_3$-labeled G, while the top panel corresponds to unlabeled O^6-Me-dG lesions that derive from guanines elsewhere in the sequence. The extent of O^6-Me-dG adduct formation at the $^{15}N_3$-labeled guanine with or without neighboring ^{Me}C can be calculated using the corresponding HPLC−MS/MS peak areas:

$$\%\ \text{reaction at } {}^{15}N_3\text{-dG} = A_{^{15}N_3-dG}/(A_{^{15}N_3-dG} + A_{^{15}N_0-dG}) \times 100\%$$

where $A_{^{15}N_3-dG}$ represents the area of the HPLC−MS/MS peak corresponding to $^{15}N_3$-labeled adducts and $A_{^{15}N_0-dG}$ represents the area of the peak corresponding to unlabeled adducts.

On the basis of the HPLC−MS/MS peak area ratios (Figure 1), the extent of O^6-Me-dG formation at codon 157 in the absence of methyl groups at the neighboring C atoms is 3.63% (panel A). The O^6-Me-dG adduct yield at the $^{15}N_3$-labeled G is decreased when ^{Me}C is placed immediately 5′ from the target guanine (2.37%, panel B) and in fully methylated dinucleotide (2.02%, panel D), but is slightly increased in the presence of a 5-methyl group at the base-paired cytosine (3.84%, panel C).

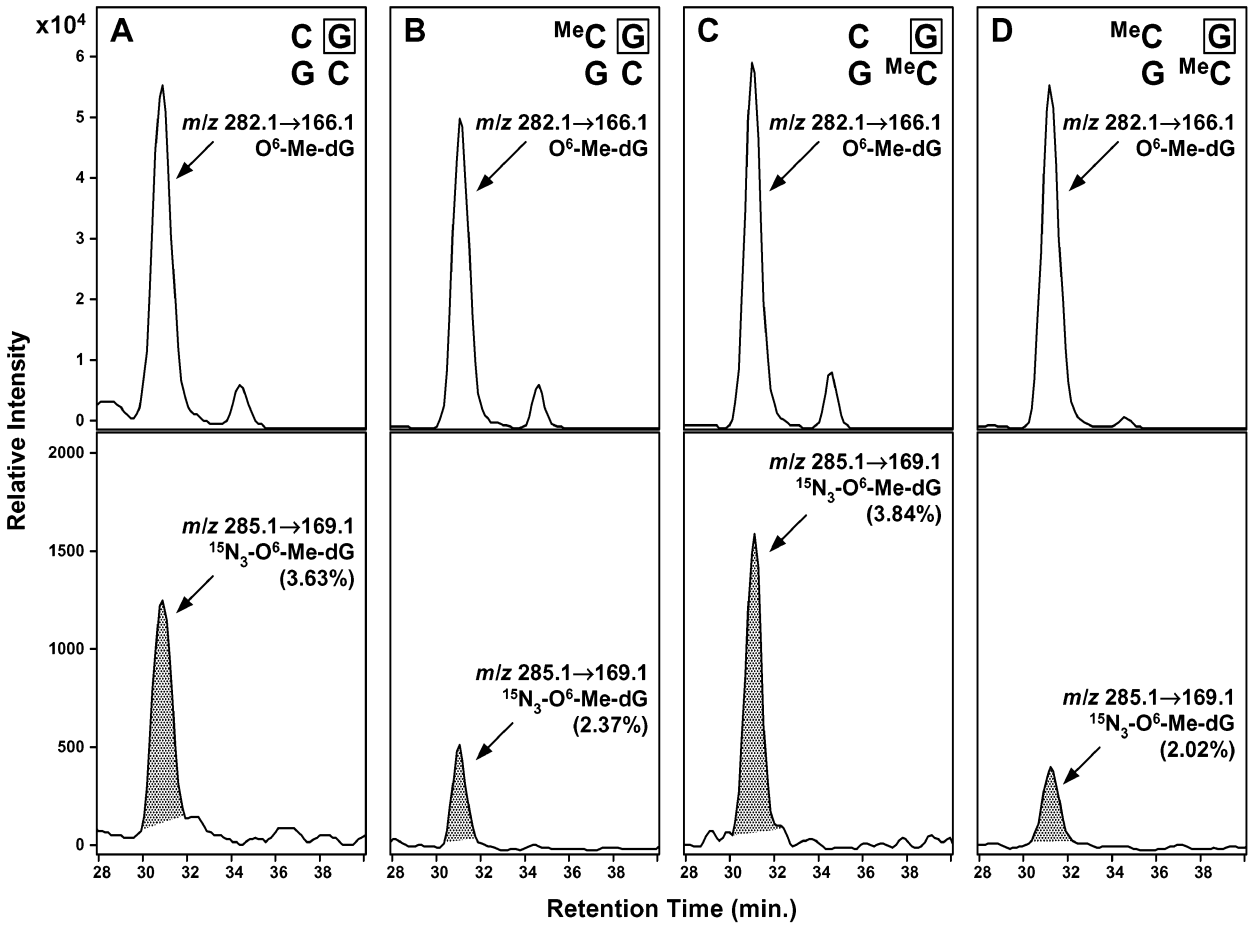

FIGURE 1: HPLC−ESI-MS/MS analysis of O^6-Me-dG (unshaded peaks) and $^{15}N_3$-O^6-Me-dG (shaded peaks) in double-stranded DNA oligonucleotide (5′-CCCGGCACCCGX$^{15}N_3$-GTCCGCG-3′, where X is C or ^{Me}C) following NDMAOAc treatment (2 mM): (A) no ^{Me}C, (B) ^{Me}C located as the 5′-neighbor to the target guanine, (C) ^{Me}C base paired with the target guanine, and (D) ^{Me}C both the 5′-neighbor to and base paired with the target guanine. For chromatography, an Agilent 1100 capillary HPLC system was used with a Zorbax SB-C18 column (150 mm × 0.5 mm, 5 μm), eluted with a gradient of 15 mM ammonium acetate (pH 5.5) (A) and 100% acetonitrile (B) at a flow rate of 15 μL/min with the following gradient: 0% B at 0−3 min, from 0 to 20% B over the course of 13.5 min, and from 20 to 40% B over the course of 2.5 min. For MS, an Agilent 1100 capillary LC−ion trap mass spectrometer (Agilent Technologies) was operated in the ESI^+ MS/MS mode (target ion abundance of 50 000, maximum accumulation time of 300 ms, three scans on average, fragmentation amplitude of 0.7, and scan width of 1.2 amu). Extracted ion chromatograms corresponding to the transitions characteristic for O^6-Me-dG (*m/z* 282.1 → 166.1) and $^{15}N_3$-O^6-Me-dG (*m/z* 285.1 → 169.1) were used for quantification.

The quantitative results for O^6-Me-dG formation in *p53* codon 157 (G^{Me}CGT sequence context, where G is $^{15}N_3$-dG) as a function of methylation status are summarized in Figure 2. Overall, the greatest effect on O^6-Me-dG adduct yields is observed in the hemimethylated duplex with ^{Me}C preceding the target guanine (30.2% reduction, $P < 0.0001$) and in the fully methylated dinucleotide (36.7% reduction, $P < 0.0001$). Adduct levels in hemimethylated duplexes following the introduction of ^{Me}C opposite the target guanine are essentially unchanged ($P > 0.8$).

A much greater inhibitory effect of ^{Me}C on guanine O^6-methylation was observed for *p53* codon 154 (C^{Me}CGG sequence context, Figure 3). As with *p53* codon 157, the preceding ^{Me}C was the most protective against O^6-alkylation (74.6% decrease in adduct yields, $P < 0.0001$). A 72.4% reduction ($P < 0.0001$) was detected when both cytosines were methylated. In contrast with our results for codon 157 (Figure 2), the base-paired ^{Me}C in codon 154 significantly decreased adduct levels at its complementary guanine (51% reduction, $P < 0.0001$; see Figure 3). When ^{Me}C was present at both positions, the O^6-Me-dG adduct yield at the labeled guanine was statistically equal to adduct yields observed in duplexes containing only the 5′-^{Me}C ($P = 1.000$).

Although the local sequence context of *p53* codon 248 is identical to that for codon 154 (C^{Me}CGG), a less pronounced reduction of O^6-Me-dG adduct levels in the presence of ^{Me}C is observed (Figure 4). As was the case for *p53* codon 154, the level of O^6-Me-dG formation in codon 248 is significantly decreased in the presence of 5′-neighboring ^{Me}C (42.9% decrease) and in fully methylated dinucleotide (43.4% reduction) (Figure 4). In addition, O^6-Me-dG formation is slightly inhibited by ^{Me}C base paired with the target guanine (18.2% inhibition, $P < 0.02$). The levels of protection imposed by 5′-^{Me}C and in fully methylated sequences were statistically equal ($P = 1.000$), suggesting that the influence of base-paired ^{Me}C is relatively minor.

Effect of ^{Me}C on the Formation of N7-Me-G Adducts by NDMAOAc (Table 2). The effect of neighboring ^{Me}C on the formation of N7-Me-G adducts was examined by HPLC−ESI-MS analysis of NDMAOAc-treated DNA following neutral thermal hydrolysis to release the N7-alkylated bases (Scheme 2). Unlike O^6-Me-dG, N7-Me-G lesions are best

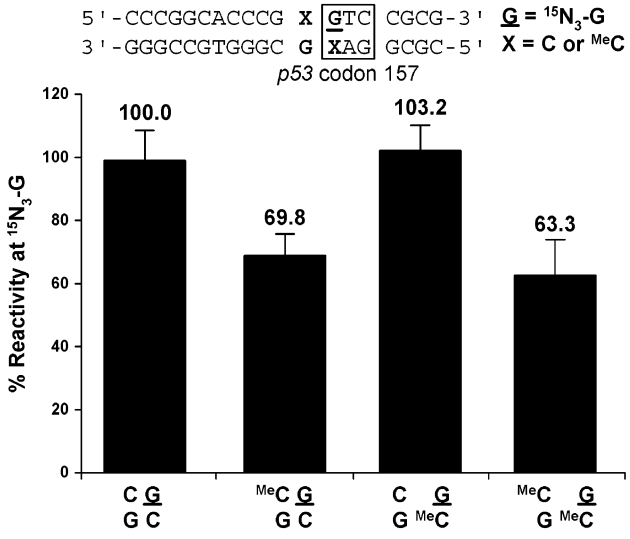

FIGURE 2: Effects of ^{Me}C on the formation of O^6-Me-dG at a CG dinucleotide within *p53* codon 157. Double-stranded oligodeoxynucleotides [5′-CCCGGCACCCG**C**G**G**TCCGCG-3′ (3−4 nmol)] containing either C or ^{Me}C adjacent to $^{15}N_3$-labeled G were treated with NDMAOAc (2 mM) in the presence of esterase, followed by HPLC−MS/MS analysis of O^6-Me-dG and $^{15}N_3$-O^6-Me-dG as described in the text. The data were compiled from three separate experiments ($N = 8-12$). Values are normalized to the amount of O^6-Me-dG formed at the $^{15}N_3$-guanine in the absence of ^{Me}C. The box indicates the codon of interest; X is C or ^{Me}C, and **G** is $^{15}N_3$-dG. See the legend of Figure 1 for HPLC−MS/MS details.

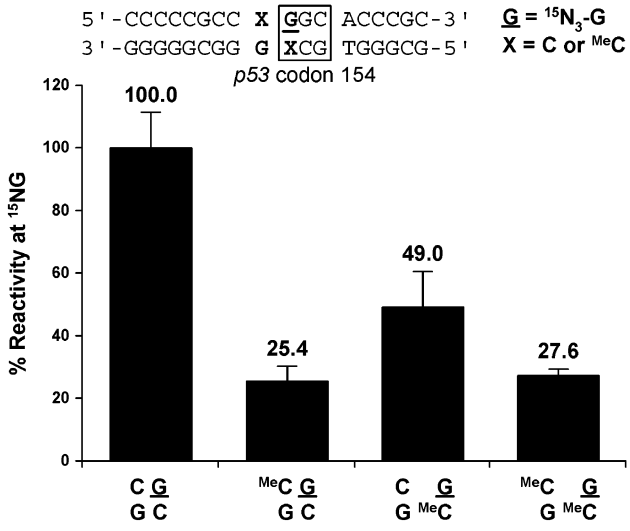

FIGURE 3: Effect of ^{Me}C on the formation of O^6-Me-dG at a CG dinucleotide derived from *p53* codon 154. Double-stranded oligodeoxynucleotides [5′-CCCCCGCC**C**G**G**CACCCGC-3′ (3−4 nmol)] containing either C or ^{Me}C adjacent to $^{15}N_3$-labeled G (**G**) were treated with NDMAOAc (2 mM) in the presence of esterase. The data were compiled from three separate experiments ($N = 4-7$). Values are normalized to the amount of O^6-Me-dG formed at the $^{15}N_3$-guanine in the absence of ^{Me}C. See the legend of Figure 1 for experimental details.

analyzed in full-scan MS mode using extracted ion chromatograms because of the lack of a predominant fragmentation pathway for the N7-Me-G base (results not shown). Our HPLC-ESI-MS analysis results indicate that the introduction of ^{Me}C only slightly inhibits the formation of N7-Me-G by NDMAOAc at all three examined *p53* gene-derived sequences (Table 2). The greatest effect (17−27% reduction) was observed in fully methylated dinucleotides ($P < 0.0001$ for all three codons). The preceding ^{Me}C alone causes a 9.5% decrease in the level of N7-Me-G formation at codon 154 ($P < 0.004$), a 17% drop at codon 157 ($P < 0.0001$), and an 11% reduction at codon 248 ($P < 0.0001$). A similar pattern (a 10−15% decrease in the level of adduct formation) is observed when the 5-methyl group is introduced at the cytosine base paired with the target guanine (Table 2).

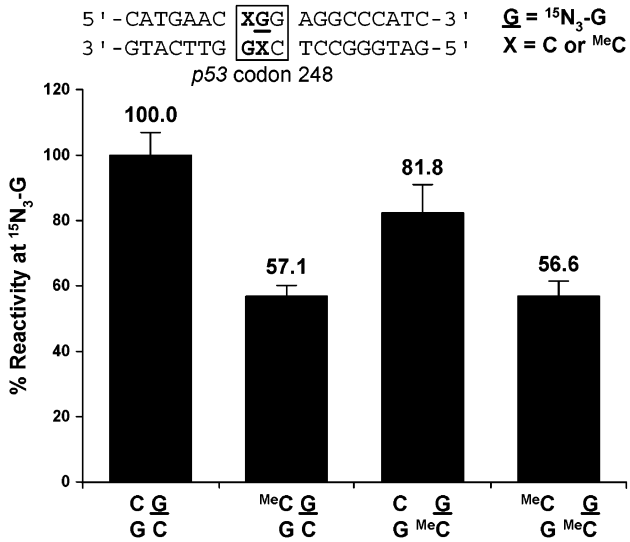

FIGURE 4: Effect of ^{Me}C on the formation of O^6-Me-dG at a CG dinucleotide derived from *p53* codon 248. Double-stranded oligodeoxynucleotides [5′-CATGAACCGGAGGCCCATC-3′ (3−4 nmol)] containing either C or ^{Me}C adjacent to $^{15}N_3$-labeled G were treated with NDMAOAc (2 mM) in the presence of esterase. The data were compiled from three separate experiments ($N = 4-6$). Values are normalized to the amount of O^6-Me-dG formed at the $^{15}N_3$-guanine in the absence of ^{Me}C. The formation of O^6-Me-dG within *p53* codon 248 is a function of cytosine methylation status. See the legends of Figures 1 and 2 for details.

Table 2: Effects of Neighboring ^{Me}C on the Formation of N7-Me-G at a Specified Guanine Base Located within *p53*-Derived DNA Sequences[a]

		5-Methylcytosine Location		
Codon	Sequence Context	^{Me}C G / G C	C G / G ^{Me}C	^{Me}C G / G ^{Me}C
154[b]	CC**G**GC[c]	90.5 ± 4.0	90.9 ± 3.1	83.4 ± 2.3
157[d]	GC**G**TC	82.9 ± 2.0	95.7 ± 3.0	72.9 ± 2.0
248[e]	C**CGG**A	89.2 ± 4.0	85.9 ± 4.1	75.2 ± 1.8

[a] Double-stranded DNA strands were treated with 2 mM NDMAOAc, and the extent of adduct formation at the underlined G was determined by stable isotope labeling HPLC−ESI-MS/MS. The values that are listed have been normalized to the percentage of N7-Me-G adducts observed at $^{15}N_3$-dG in the absence of ^{Me}C. [b] $N = 5-7$. [c] G is $^{15}N_3$-dG; the underlined text represents the indicated codon. [d] $N = 5$. [e] $N = 7-9$.

Effects of ^{Me}C on the Formation of O^6-POB-dG Adducts in p53 Codon 157. Guanine modification by NNK-derived [4-oxo-4-(3-pyridyl)but-1-yl]diazohydroxide gives rise to O^6-POB-dG adducts (Scheme 1). If the observed inhibition of O^6-Me-dG formation by ^{Me}C (Figures 2−4) occurs by a steric mechanism, an even greater effect is expected for O^6-POB-dG because of the larger site of POB diazohydroxide (Scheme 1). We examined the effects of ^{Me}C on the formation of O^6-POB-dG lesions in double-stranded synthetic oligo-

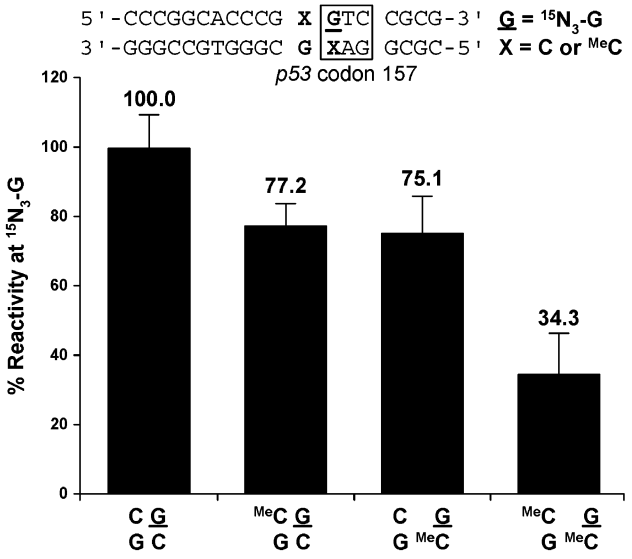

FIGURE 5: Effect of ^{Me}C on the formation of O^6-POB-dG at a 5′-CG dinucleotide derived from *p53* codon 248 ($N = 3$). Double-stranded oligodeoxynucleotides [5′-CCCCCGCC**CG**GCACCCGC-3′, (+) strand (5 nmol)] containing either C or ^{Me}C adjacent to $^{15}N_3$-labeled G were treated with NNKOAc (5 mM) in the presence of esterase. An Agilent 1100 capillary LC−ion trap system was operated in the ESI$^+$ mode with nitrogen as a nebulizing (15 psi) and drying gas (5 L/min, 200 °C). Quantitative analysis was achieved by MS/MS analysis of O^6-POB-dG (m/z 415.4 → 299.1) and $^{15}N_3$-O^6-POB-dG (m/z 418.4 → 302.1). The target ion abundance value was set to 30 000; the maximum accumulation time was 300 ms, and three scans were taken on average.

deoxynucleotides representing *p53* codon 157 and the surrounding sequence (Figure 5). The experimental approach was similar to the methods employed for O^6-Me-dG analyses (see above). In analogy with O^6-Me-dG, the formation of O^6-POB-dG was inhibited in the presence of ^{Me}C (Figure 5). The magnitude of the reduction of O^6-POB-dG yields in the presence of a 5′-neighboring ^{Me}C was similar to the effect observed for O^6-methylation in the same sequence (23 vs 30%; see Figures 5 and 2, respectively). However, ^{Me}C in the opposite strand reduced the level of O^6-guanine pyridyloxobutylation, but not O^6-G methylation (compare Figures 5 and 2), suggesting that base-paired ^{Me}C may hinder the pyridyloxobutylation of O^6-G by blocking the access of the bulky alkylating agent. In contrast, the 5′-neighboring ^{Me}C reduces the reactivity of guanine toward both methylating and pyridyloxobutylating species by an alternative mechanism not involving steric factors. As expected, the most pronounced decrease in O^6-POB-dG adduct yields occurred in fully methylated dinucleotides (65.7% decrease, $P < 0.0003$) (Figure 5), suggesting that ^{Me}C residues at the two positions of CG dinucleotides have an additive effect in protecting the target guanine against pyridyloxobutylation by NNK metabolite.

^{Me}C Shifts O^6-Me-dG/N7-Me-G Adduct Ratios. The observed reduction in O^6-guanine adduct yields in methylated CG dinucleotides may result from an altered regioselectivity for guanine alkylation, leading to a smaller contribution of the O^6 lesions to the total adduct numbers. To test this hypothesis, we analyzed the effects of cytosine C5 methylation on O^6-Me-dG/N7-Me-G adduct ratios in *p53* codon 154 (Figure 6). *p53* codon 154 was selected for this analysis because ^{Me}C at this site affords a high degree of protection against O^6-guanine methylation (Figure 3). The molar ratio

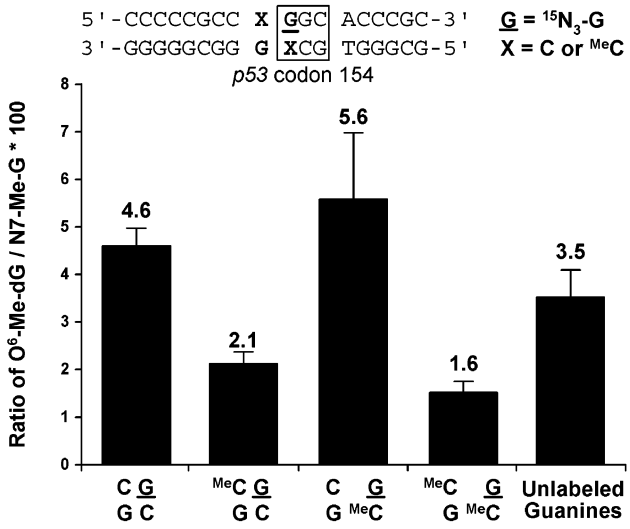

FIGURE 6: O^6-Methylguanine/N7-methylguanine molar ratios as a function of neighboring ^{Me}C in *p53* codon 154. Double-stranded oligonucleotides (3 nmol) containing *p53* codon 154 were treated with 2 mM NDMAOAc, and the resulting methylguanine adducts originating from $^{15}N_3$-labeled and unlabeled guanines were analyzed by HPLC−ESI-MS/MS (O^6-Me-dG) and HPLC−ESI-MS (N7-Me-G). Calibration curves for the quantification of both O^6-Me-dG and N7-Me-G were constructed using standard solutions of both adducts ($R^2 = 0.994$ for O^6-Me-dG, and $R^2 = 0.990$ for N7-Me-G) ($N = 3$).

of the O^6- and N7-methylguanines originating from $^{15}N_3$-labeled G within codon 154 containing no ^{Me}C was 4.6% (Figure 6), while the average O^6-Me-dG/N7-Me-G molar ratio for this sequence was 3.5% as determined by an independent quantification of the corresponding unlabeled lesions (Figure 6). Placement of ^{Me}C immediately 5′ from $^{15}N_3$-G and in both positions of the 5′-C-$^{15}N_3$-G-3′ dinucleotide significantly decreased the O^6-Me-dG/N7-Me-G molar ratio [O^6-Me-dG/N7-Me-G ratio of 2.1% ($P < 0.02$) and 1.5% ($P < 0.0001$), respectively]. In contrast, ^{Me}C in the opposite strand slightly increased the extent of O^6-G alkylation, although this effect was not statistically significant ($P > 0.9$; Figure 6). These results indicate that 5′-neighboring ^{Me}C shifts the reactivity patterns of the target G, leading to a less efficient methylation of the O^6-guanine position.

DISCUSSION

More than 35% of all human cancers and approximately 60% of human lung cancers contain mutations in the *p53* tumor suppressor gene (*12*, *21*). The majority of *p53* mutations are found in sequences that encode amino acids in the DNA binding domain of the *p53* protein (exons 5, 7, and 8) (*12*). Interestingly, many of these mutational hot spots are located at endogenously methylated CG sites (*11*, *18*, *19*, *23*). It has been proposed that *p53* mutational hot spots observed in smoking-induced lung cancer are the result of an enhanced reactivity of guanines within methylated CG dinucleotides toward benzo[*a*]pyrene diol epoxide (BPDE) and other PAH diol epoxides (*22*, *23*, *49*). Using a *uvr*ABC incision assay in combination with LMPCR, these authors have demonstrated that the hot spots for BPDE-induced DNA damage correspond to *p53* mutational hot spots observed in lung tumors from smokers (*49*). Since the characteristic hot spots for PAH-induced DNA damage were observed only in the physiologically methylated *p53* gene, enhanced adduct

formation at these sites has been attributed to the effects of neighboring ^{Me}C (*22*, *24*). Our laboratory used stable isotope labeling HPLC−ESI-MS/MS to demonstrate that ^{Me}C located across from the target guanine increases the yields of BPDE−N^2-guanine adducts 2−2.5-fold as compared to the yield of adduct formation in the absence of ^{Me}C (*45*).

Several alternative explanations can be put forward to account for the enhanced BPDE−N^2-dG adduct formation at endogenously methylated CG dinucleotides (*50*, *51*). *In vivo* methylation of CG sites introduces two ^{Me}C nucleobases (one in each DNA strand), both of which may affect the reactivity of the neighboring guanines. The nucleophilicity of the N^2 position of guanine has been proposed to be increased as a result of electron donating effects of the 5-methyl group of ^{Me}C transmitted through the ^{Me}C·G base pair (*50*). *Ab initio* calculations suggest that methylated cytosine may act as a base catalyst, increasing the reactivity of the N^2 position of guanine toward electrophiles (*52*). Alternatively, ^{Me}C may facilitate hydrophobic interactions between DNA and PAH diol epoxides (*51*). For example, stacking of the pyrenyl group of BPDE with ^{Me}C in the opposite strand (*51*) may favorably position the epoxy ring of BPDE for nucleophilic attack by the N^2-amino group of the base-paired guanine.

In sharp contrast with the existing data for PAH diol epoxides, our experiments reported herein (Table 2 and Figures 1−5) demonstrate that ^{Me}C at *p53* codons 157, 154, and 248 inhibit the formation of NNK-induced N-7- and O^6-guanine adducts at neighboring G residues. The extent of ^{Me}C-induced protection ranges from 17−27% for N7-Me-G adducts to 65−75% for O^6-Me-dG and O^6-POB-dG lesions. This effect is modulated by the local sequence context and by the actual nature of the DNA alkylating species, with the greatest protection observed in the CC ^{Me}CGGC sequence (*p53* codon 154; see Figure 3). Our findings are in accord with previous reports by Mathison *et al.* (*30*) and Sendowski and Rajewsky (*29*), who observed a reduction of N7-Me-G and O^6-Me-dG adduct yields in synthetic oligomers with repeating sequence upon incorporation of ^{Me}C. We saw a similar protective effect of ^{Me}C against O^6-pyridyloxobutylation (Figure 5), suggesting that this may be a general phenomenon for O^6-guanine alkylation. Our results for codon 248 contradict the earlier study by Ross and collaborators (*53*), who reported that N7-Me-G yields are not affected by ^{Me}C. This discrepancy can be rationalized by the use of different methylating agents (dimethyl sulfate vs methyldiazohydroxide) and different detection methods (mass spectrometry of DNA hydrolysates vs gel electrophoresis of hot piperidine-cleaved DNA) (*53*). NNK diazohydroxides produce positively charged diazonium ions and/or carbocations that are likely to have different DNA sequence preferences than electrically neutral DMS.

The stable isotope labeling HPLC−MS approach directly quantifies the relative reactivity of selected guanine nucleobases within a gene sequence with and without 5-methyl substituents at the neighboring cytosines. Therefore, it enables us to independently analyze the effects of ^{Me}C in the same strand and in the opposite strand from the target G. We found that the maximum protection against N7- and O^6-alkylation is achieved in fully methylated sequences, with the 5′-neighboring ^{Me}C having the greatest contribution to this effect (Figures 2−5). In all three *p53* codons that were examined, O^6-guanine reactivity toward the methylating agent was statistically the same in fully methylated dinucleotides as in sequences containing ^{Me}C exclusively at the 5′-neighboring position (Figures 2−4).

The differing effect of neighboring ^{Me}C on guanine reactions with PAH diol epoxides and NNK-derived diazohydroxides is not totally unexpected. Unlike PAHs, NNK-derived DNA reactive species (Scheme 1) lack the fused aromatic ring structure required for the formation of intercalated complexes. Furthermore, the methylating and pyridyloxobutylating species of NNK (e.g., diazonium ions and/or carbocations) may bear a positive charge (Scheme 1); if so, their interactions with DNA may be strongly influenced by any local changes in the charge density of the phosphodiester backbone in the presence of ^{Me}C. Finally, PAH diol epoxides and NNK diazohydroxides target different sites within guanine (N^2 and O^6, respectively), which may be affected by neighboring ^{Me}C in a different way.

The presence of ^{Me}C in poly(dG-^{Me}C) sequences has been shown to alter the structural and energetic properties of the double helix (*54*), stabilizing the Z form of DNA (*55*, *56*), although the effect of a single-site cytosine C5 methylation on DNA structure is relatively minor (*57*, *58*). Our results for a sequence containing *p53* codon 157 reveal that ^{Me}C in the opposite strand decreases the extent of O^6-pyridyloxobutylation, but has no effect on O^6-methylguanine adduct formation (see Figures 2 and 5). Since the pyridyloxobutylating species (POB diazohydroxide) is larger than the methylating agent (Me diazohydroxide), this observation is consistent with a steric hindrance by ^{Me}C in the opposite strand. In contrast, similar reductions of the O^6-methyl and O^6-pyridyloxobutyl adduct yields by 5′-neighboring ^{Me}C argue against steric effects of 5′-neighboring ^{Me}C on the reactivity of O^6-guanine.

A partial explanation for the observed protective effects of preceding ^{Me}C on O^6-guanine alkylation by NNK metabolites is provided by the shifted reactivity patterns in methylated CG dinucleotides. A 2.5-fold reduction in the O^6-Me-dG/N7-Me-G molar ratio is observed in the presence of 5′-neighboring ^{Me}C (Figure 6). This may be caused by local helical disruptions in the presence of ^{Me}C, leading to a decreased accessibility and/or altered charge density in the vicinity of the O^6 position of guanine. Alternatively, electronic effects of ^{Me}C transmitted through the ^{Me}C·G base pair may facilitate electrophilic attack at an alternative site within guanine. For example, theoretical studies predict that the nucleophilicity of the N^2 position of guanine in methylated CG dinucleotides is increased as a result of hydrogen bond acid/base catalysis involving the C═O group of the cytosine (*52*). Studies are in progress at our laboratory to test the effects of ^{Me}C on the formation of recently reported N^2-pyridyloxobutylguanine adducts of NNK (*59*).

In summary, our results indicate that, unlike N^2-guanine adducts of PAH diol epoxides, NNK-induced N7- and O^6-guanine lesions are not preferentially formed at endogenously methylated CG sites within the *p53* tumor suppressor gene. On the contrary, neighboring ^{Me}C reduces the extent of formation of promutagenic O^6-Me-dG and O^6-POB-dG lesions at methylated CG dinucleotides, potentially leading to an overall protective effect against NNK mutagenesis. These results are consistent with a relatively low frequency of G to A transitions at methylated CG dinucleotides within

the *p53* tumor suppressor gene in smoking-induced lung cancer (*12*). However, a concurrent weakening of the ability of O^6-alkylguanine DNA alkyltransferase to repair O^6-alkylguanine lesions when they are preceded 5′ by ^{Me}C (*60*) may lead to their accumulation at methylated CG sites. Furthermore, cytosine C5 methylation may promote the formation of minor NNK−guanine adducts not examined in this work (e.g., N^2-POB-dG). Therefore, NNK-induced DNA damage cannot be ruled out as a factor contributing to *p53* mutagenesis in smoking-induced lung cancer.

ACKNOWLEDGMENT

We thank Prof. Lisa Peterson at the University of Minnesota Cancer Center (Minneapolis, MN) for the O^6-pyridyloxobutyldeoxyguanosine standard, Prof. Stephen Hecht (University of Minnesota) for helpful discussions and detailed comments on the manuscript, Susan Schulte (University of Minnesota Cancer Center Biostatistics Core, Minneapolis, MN) for statistical analyses of our data, Gregory Janis for editorial help, and Agilent Technologies for providing the 1100 capillary LC−ion trap MS system.

REFERENCES

1. Ehrlich, M., Gama-Sosa, M. A., Huang, L. H., Midgett, R. M., Kuo, K. C., McCune, R. A., and Gehrke, C. (1982) *Nucleic Acids Res. 10*, 2709−2721.
2. Riggs, A. D., and Jones, P. A. (1983) *Adv. Cancer Res. 40*, 1−30.
3. Bird, A. P. (1986) *Nature 321*, 209−213.
4. Tate, P. H., and Bird, A. P. (1993) *Curr. Opin. Genet. Dev. 3*, 226−231.
5. Schroeder, M., and Mass, M. J. (1997) *Biochem. Biophys. Res. Commun. 235*, 403−406.
6. Newell-Price, J., Clark, A. J., and King, P. (2000) *Trends Endocrinol. Metab. 11*, 142−148.
7. Ballestar, E., and Esteller, M. (2002) *Carcinogenesis 23*, 1103−1109.
8. Momparler, R. L., and Bovenzi, V. (2000) *J. Cell. Physiol. 183*, 145−154.
9. Warnecke, P. M., and Bestor, T. H. (2000) *Curr. Opin. Oncol. 12*, 68−73.
10. Tornaletti, S., and Pfeifer, G. P. (1995) *Oncogene 10*, 1493−1499.
11. Pfeifer, G. P., Denissenko, M. F., Olivier, M., Tretyakova, N., Hecht, S. S., and Hainaut, P. (2002) *Oncogene 21*, 7435−7451.
12. Greenblatt, M. S., Bennett, W. P., Hollstein, M., and Harris, C. C. (1994) *Cancer Res. 54*, 4855−4878.
13. Conway, K., Edmiston, S. N., Cui, L., Drouin, S. S., Pang, J., He, M., Tse, C. K., Geradts, J., Dressler, L., Liu, E. T., Millikan, R., and Newman, B. (2002) *Cancer Res. 62*, 1987−1995.
14. Shen, J. C., Rideout, W. M., III, and Jones, P. A. (1994) *Nucleic Acids Res. 22*, 972−976.
15. Rideout, W. M., III, Coetzee, G. A., Olumi, A. F., and Jones, P. A. (1990) *Science 249*, 1288−1290.
16. Jones, P. A., Buckley, J. D., Henderson, B. E., Ross, R. K., and Pike, M. C. (1991) *Cancer Res. 51*, 3617−3620.
17. Cooper, D. N., and Youssoufian, H. (1988) *Hum. Genet. 78*, 151−155.
18. Pfeifer, G. P. (2000) *Mutat. Res. 450*, 155−166.
19. Hainaut, P., and Pfeifer, G. P. (2001) *Carcinogenesis 22*, 367−374.
20. Husgafvel-Pursiainen, K., and Kannio, A. (1996) *Environ. Health Perspect. 104* (Suppl. 3), 553−556.
21. Bennett, W. P., Hussain, S. P., Vahakangas, K. H., Khan, M. A., Shields, P. G., and Harris, C. C. (1999) *J. Pathol. 187*, 8−18.
22. Denissenko, M. F., Chen, J. X., Tang, M. S., and Pfeifer, G. P. (1997) *Proc. Natl. Acad. Sci. U.S.A. 94*, 3893−3898.
23. Smith, L. E., Denissenko, M. F., Bennett, W. P., Li, H., Amin, S., Tang, M., and Pfeifer, G. P. (2000) *J. Natl. Cancer Inst. 92*, 803−811.
24. Chen, J. X., Zheng, Y., West, M., and Tang, M. S. (1998) *Cancer Res. 58*, 2070−2075.
25. Li, V. S., Reed, M., Zheng, Y., Kohn, H., and Tang, M. (2000) *Biochemistry 39*, 2612−2618.
26. Parker, B. S., Cutts, S. M., and Phillips, D. R. (2001) *J. Biol. Chem. 276*, 15953−15960.
27. Mathur, P., Xu, J., and Dedon, P. C. (1997) *Biochemistry 36*, 14868−14873.
28. Hertzberg, R. P., Caranfa, M. J., and Hecht, S. M. (1985) *Biochemistry 24*, 5286−5289.
29. Sendowski, K., and Rajewsky, M. F. (1991) *Mutat. Res. 250*, 153−160.
30. Mathison, B. H., Said, B., and Shank, R. C. (1993) *Carcinogenesis 14*, 323−327.
31. Hecht, S. S. (1999) *Mutat. Res. 424*, 127−142.
32. Singer, B., and Grunberger, D. (1983) *Molecular Biology of Mutagens and Carcinogens*, Plenum Press, New York.
33. Loechler, E. L., Green, C. L., and Essigmann, J. M. (1984) *Proc. Natl. Acad. Sci. U.S.A. 81*, 6271−6275.
34. Pauly, G. T., Peterson, L. A., and Moschel, R. C. (2002) *Chem. Res. Toxicol. 15*, 165−169.
35. Liu, X. K., Spratt, T. E., Murphy, S. E., and Peterson, L. A. (1996) *Chem. Res. Toxicol. 9*, 949−953.
36. Peterson, L. A., Liu, X. K., and Hecht, S. S. (1993) *Cancer Res. 53*, 2780−2785.
37. Peterson, L. A., Thomson, N. M., Crankshaw, D. L., Donaldson, E. E., and Kenney, P. J. (2001) *Cancer Res. 61*, 5757−5763.
38. Belinsky, S. A., Foley, J. F., White, C. M., Anderson, M. W., and Maronpot, R. R. (1990) *Cancer Res. 50*, 3772−3780.
39. Peterson, L. A., and Hecht, S. S. (1991) *Cancer Res. 51*, 5557−5564.
40. Hecht, S. S. (1998) *Chem. Res. Toxicol. 11*, 559−603.
41. Gentil, A., Cabral-Neto, J. B., Mariage-Samson, R., Margot, A., Imbach, J. L., Rayner, B., and Sarasin, A. (1992) *J. Mol. Biol. 227*, 981−984.
42. Takeshita, M., and Eisenberg, W. (1994) *Nucleic Acids Res. 22*, 1897−1902.
43. Avkin, S., Adar, S., Blander, G., and Livneh, Z. (2002) *Proc. Natl. Acad. Sci. U.S.A. 99*, 3764−3769.
44. Kunkel, T. A. (1984) *Proc. Natl. Acad. Sci. U.S.A. 81*, 1494−1498.
45. Tretyakova, N., Matter, B., Jones, R., and Shallop, A. (2002) *Biochemistry 41*, 9535−9544.
46. Ziegel, R., Shallop, A., Jones, R., and Tretyakova, N. (2003) *Chem. Res. Toxicol. 16*, 541−550.
47. Sansone, E. B., and Tewary, Y. B. (1978) *The Permeability of Laboratory Gloves to Selected Nitrosamines*, International Agency for Research on Cancer, Lyon, France.
48. Wang, L., Spratt, T. E., Liu, X. K., Hecht, S. S., Pegg, A. E., and Peterson, L. A. (1997) *Chem. Res. Toxicol. 10*, 562−567.
49. Denissenko, M. F., Pao, A., Tang, M., and Pfeifer, G. P. (1996) *Science 274*, 430−432.
50. Das, A., Tang, K. S., Gopalakrishnan, S., Waring, M. J., and Tomasz, M. (1999) *Chem. Biol. 6*, 461−471.
51. Geacintov, N. E., Shahbaz, M., Ibanez, V., Moussaoui, K., and Harvey, R. G. (1988) *Biochemistry 27*, 8380−8387.
52. Dannenberg, J. J., and Tomasz, M. (2000) *J. Am. Chem. Soc. 122*, 2062−2068.
53. Ross, M. K., Mathison, B. H., Said, B., and Shank, R. C. (1999) *Biochem. Biophys. Res. Commun. 254*, 114−119.
54. Zacharias, W., O'Connor, T. R., and Larson, J. E. (1988) *Biochemistry 27*, 2970−2978.
55. Behe, M., and Felsenfeld, G. (1981) *Proc. Natl. Acad. Sci. U.S.A. 78*, 1619−1623.
56. Fujii, S., Wang, A. H., van der, M. G., van Boom, J. H., and Rich, A. (1982) *Nucleic Acids Res. 10*, 7879−7892.
57. Heinemann, U., and Hahn, M. (1992) *J. Biol. Chem. 267*, 7332−7341.
58. Frederick, C. A., Saal, D., van der Marel, G. A., van Boom, J. H., Wang, A. H., and Rich, A. (1987) *Biopolymers 26* (Suppl.), S145−S160.
59. Wang, M., Cheng, G., Sturla, S. J., Shi, Y., McIntee, E. J., Villalta, P. W., Upadhyaya, P., and Hecht, S. S. (2003) *Chem. Res. Toxicol. 16*, 616−626.
60. Bentivegna, S. S., and Bresnick, E. (1994) *Cancer Res. 54*, 327−329.

BI035259J